PHYSICAL REVIEW B VOLUME 15, NUMBER 2 15 JANUARY 1977

Angular-dependent x-ray-photoelectron peak intensities from single-crystal gold

R. J. Baird, C. S. Fadley,[†] and L. F. Wagner
Department of Chemistry, University of Hawaii, Honolulu, Hawaii 96822

(Received 9 February 1976; revised manuscript received 12 July 1976)

Detailed measurements of the angular distributions of x-ray-photoelectron intensities from a gold single crystal are reported. The energy-integrated $4d$-, $4f$-, and valence-peak intensities exhibit essentially identical angular distributions consistent with the near equality of their corresponding photoelectron de Broglie wavelengths. A $4f$ intensity contour plot over the full 2π solid angle is found to agree very well with the qualitative predictions of Kikuchi-band theory. The relationship of such effects to angular-dependent changes in valence-spectrum fine structure observed previously is also discussed.

I. INTRODUCTION

Pronounced fine structure has been observed previously in the angular distributions of core- and valence-x-ray-photoelectron (XPS) peak intensities from single crystals of NaCl,[1] Au,[2-4] KCl,[5] and Si.[4,6,7] These effects are associated with electron diffraction phenomena, and lead to enhanced emission along certain directions fixed with respect to the crystal axes. However, the data reported in prior studies have been limited to one,[1,4-6] or at most a few,[2] distinct polar-angle scans for a given crystal, and relatively large angular intervals of ~5° have also been used in some aspects of these investigations.[2] In addition, although previous discussions[1,2,4,5,8] have implied the connection of such phenomena with the Kikuchi bands observed, for example, in low-energy-electron diffraction (LEED) experiments carried out at kinetic energies ≳300 eV,[9] no detailed comparisons of experimental intensities with the well-established systematics of these bands have been made. In this paper, we report the most extensive measurements of this type performed to date, including polar plots of core- and valence-angular distributions and the first detailed intensity contour plot over essentially the full 2π solid angle. The intensity contours are furthermore compared with the qualitative expectations of Kikuchi-band theory. The relationship of such effects to the strong angular dependence noted previously in the relative intensities of various features in XPS valence spectra from single crystals[3,4] is also discussed qualitatively.

II. EXPERIMENTAL PROCEDURE

Measurments were performed on a Hewlett Packard 5950A spectrometer which had been modified to permit computer-controlled *in situ* two-axis rotation of the specimen.[4,10] A schematic drawing of the experimental geometry is shown in Fig. 1. Both the polar angle θ and the azimuthal angle ϕ associated with the electron emission direction from the surface were varied. (θ is here defined such that 90° corresponds to emission perpendicular to the surface.) An accuracy of ±1° was obtained in both angles. The solid angle accepted by the analyzer has been determined by electron-trajectory calculations to be a cone of 3.5° half angle.[10] The angle between the x-ray-incidence and electron-exit directions was fixed such that $\alpha = 72°$ in Fig. 1, and polar rotations were performed about an axis perpendicular to the plane containing these directions. Azimuthal rotations were about the surface normal. Monochromatized Al $K\alpha$ radiation was used for excitation. Peak intensities from this spectrometer have previously been shown to vary significantly with polar angle according to a well-defined instrument response function.[4,10,11] If normalized to $\theta = 90°$, this smoothly varying function has values of 1.00 at 90°, 0.74 at 70°, 0.47 at 50°, 0.27 at 30°, 0.09 at 10°, and zero at 0°.

A gold single crystal was mechanically polished and etched with aqua regia to remove surface disorder. The surface normal was oriented 8 ± 1° away from [001] along a direction toward [$\bar{1}\bar{1}1$]. (This orientation permitted the determination of valence-spectrum fine structure along several ⟨100⟩ and ⟨110⟩ directions[3,4] by avoiding grazing exit angles for which the response function is zero.) All measurments in the photoelectron spectrometer were performed at 25–28 ℃ and at pressures of $(2-4)\times 10^{-9}$ Torr. Carbon was the only surface contaminant observed, with the C $1s$ to Au $4f$ intensity ratio being 0.03–0.04 and thus indicative of a coverage of 1–2 monolayers.[12] An amorphous carbon overlayer was also suggested by the structureless C $1s$ angular distributions observed. Prior studies[2,4,6] indicate that such an overlayer should have a negligible smearing effect on the gold photoelectron angular distributions. The surface order of the gold crystal was verified by LEED experiments in a separate system; these

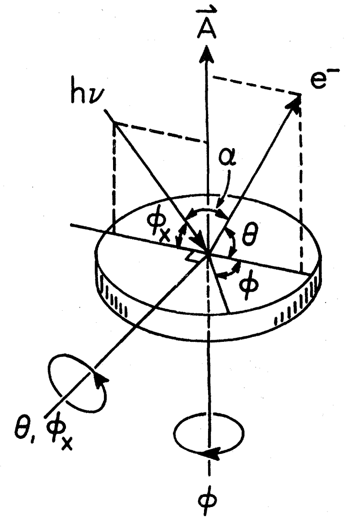

FIG. 1. Schematic illustration of the experimental geometry, with various pertinent angles defined. Rotation of the specimen on both axes noted was possible. The angle α was fixed at 72°.

gave spot patterns characteristic of the (001) surface after only light ion bombardment to remove the carbon present. Subsequent annealing did not change the LEED results.

The mean kinetic energies and de Broglie wavelengths associated with the gold peaks studied are Au $4d_{3/2,5/2}$—1140 eV, 0.363 Å; Au $4f_{5/2,7/2}$—1397 eV, 0.328 Å; and Au valence—1471–1481 eV, 0.319–0.318 Å. Peak intensities were determined as integrated areas above linear backgrounds, thus eliminating any effects due to angle-dependent resolution changes in the spectrometer.[10] The XPS valence-peak intensities for gold are well-known to be associated primarily with the $5d$ bands.

Polar-angle scans were made for the $4d$, $4f$, and valence spectral regions along several planes. Also, the $4f$ spectral region was singled out for more detailed study and intensity determinations were made over the full solid angle on a grid with angular intervals of $\Delta\theta = 2.7°$ and $\Delta\phi = 3.0$. The data were accumulated in two overlapping ϕ scans of 210° each, between which the specimen was removed from the spectrometer for manual rotation by 180°. The approximately 4000 data points so obtained were then used to derive contours of equal intensity via a two-dimensional Laplacian interpolation scheme. Minimal data smoothing was involved in generating these contours.

III. RESULTS AND DISCUSSION

A. Energy-integrated intensities and Kikuchi effects

Angular distributions for the $4d$, $4f$, and valence peaks are shown in Fig. 2 for two separate polar-angle scans. The angle interval used was 2.7°. Curves A correspond to scanning the emission direction approximately in a $(1\bar{1}0)$ plane containing the [001] and [111] directions and curves B to a scan approximately in a (100) plane containing the [001] and [011] directions.[13] All curves are modulated by the instrument response function as quoted. Significant features common to the sets of curves are labeled, with peaks 5 and 10 corresponding to emission along [001]. Although the curves for the two different polar scans are markedly different in shape, it is clear from this data that the angular distributions for all three spectral regions in a given scan are essentially identical. Features 1–10 have very nearly the same positions, relative intensities, and widths for all three curves. This agreement includes very narrow structures such as 4, 7, and 9, which have total base widths of only ~5°. Such correspondence between angular distributions is consistent with previous data of lower accuracy and resolution obtained by Fadley and Bergström.[2] Such results thus suggest scattering effects that are dominated by the final-state character of the photoelectron, as the de Broglie wavelengths associated with the

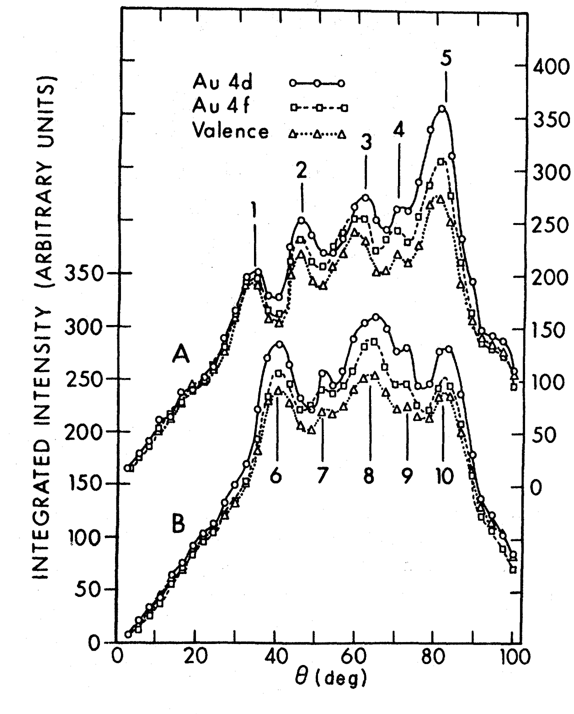

FIG. 2. XPS total peak intensities for Au $4d$, Au $4f$, and Au valence levels as a function of polar emission angle from a single crystal with very nearly [001] orientation. θ is defined such that 90° represents emission along the surface normal, and peaks 5 and 10 occur for electron emission along the [001] direction. Results for two different polar-angle scans are shown, with A passing through the [001] and [111] directions and B including the [001] and [011] directions.

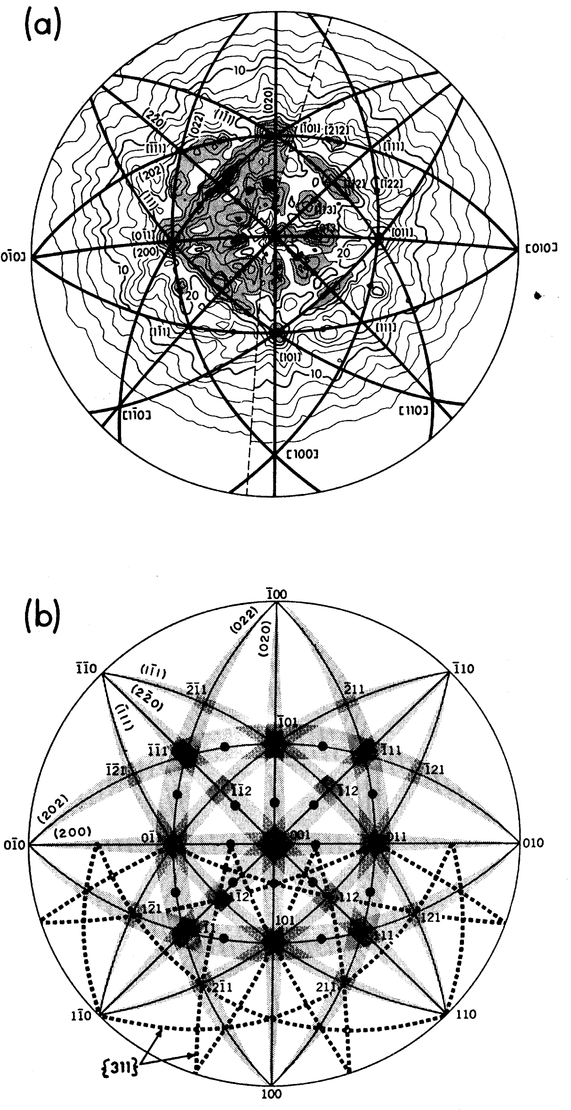

FIG. 3. (a) Experimental Au $4f$ XPS intensity contours for the single crystal of Fig. 2, shown in stereographic projection. The dotted lines distinguish two sets of data with slightly different total intensities. Various low-index directions and planes are labeled, with [001] offset 9° vertically from the center. Intensity contours are expressed in arbitrary units, with those for 10 and 20 labeled; regions between 22 and 30 are shaded, and regions above 30 are shown in black. (b) Qualitative predictions of Kikuchi-band theory for the Au $4f$ intensity distribution, also in stereographic projection. Shaded bands $2\theta_{hkl}$ wide are shown for the principal low-index planes {111}, {200}, and {220}. The dotted lines in the lower half of the figure indicate the locations of the centers of the bands associated with the higher-index {311} planes; the equivalent bands in the upper half are related by reflection symmetry. Low-index directions are indicated either by specific labels or, for ⟨310⟩, ⟨311⟩, and ⟨221⟩, by dots at points corresponding to those shown in (a).

$4d$, $4f$, and valence peaks differ by at most 13%. Initial-state properties such as the degree of localization of the orbital from which photoemission occurs thus do not appear to play a major role in determining these angular distributions of integrated peak intensity, even though we have also previously observed[3,4] that the relative intensities of various components within the gold valence-band spectrum change by ~±15% for different electron-emission directions in the crystal. The relationship of such valence-spectrum relative-intensity changes to total-intensity angular distributions is discussed in Sec. III B.

The $4f$ intensity contour results are presented in stereographic projection in Fig. 3(a), in which various low-index directions and planes are labeled. (The location of the [001] direction is obvious, and the surface normal is oriented 8° away from it towards [$\bar{1}\bar{1}1$].) The dotted lines separate data obtained in the two different ϕ scans. Due to slight instrumental intensity drifts and possible small changes in surface contaminant levels during external rotation between ϕ scans, the two sets of data show slightly different average intensities; these differences are never greater than 25% between points with corresponding symmetry, however. No correction has been made for the instrument response function, so intensities generally decrease as the polar orientation moves away from the surface normal. An additional intensity decrease occurs toward low θ because of attenuation in the thin contaminant overlayer,[11,12] and it is because of the difficulty of accurately allowing for this effect that no attempt was made to correct the data by dividing out the response function.

The contours of Fig. 3(a) clearly exhibit the fourfold symmetry of the (001) surface, with regions of highest intensity occurring along various low-index directions (or equivalently, along the intersections of several low-index planes). In particular, intensity maxima are found along the [001], ⟨110⟩, and ⟨211⟩ directions and also lie very close to the ⟨221⟩, ⟨310⟩, and ⟨311⟩ directions.[13] The outer, approximately circular, contours (such as those labeled "10") also exhibit symmetric structures that are suggestive of bands of higher intensity lying along low-index planes [as, for example, (1$\bar{1}$1), (2$\bar{2}$0), and (111)]. By comparing Figs. 2 and 3(a), it can also be seen that several peaks occur very close to certain low-index directions: peaks 1 lie along [111], peaks 2 along [112], and peaks 6 along [011].

An explanation of these effects in terms of the known phenomenology of Kikuchi bands[8,9] requires that each set of planes hkl has associated with it a band of excess intensity oriented parallel to the planes and possessing an angular width of approximately $2\theta_{hkl}$, with θ_{hkl} being the Bragg angle for electron diffraction from the planes. These bands may be bordered by deficiency regions of much smaller angular widths, and may also exhibit intensity minima at their centers.[8,9] For the three lowest-index planes in the fcc gold crystal from which diffraction is allowed, the Bragg angles for $4f$ photoelectrons are {111}—4.0°, {200}—4.6°, and {220}—6.5°. As a simple test of the qualitative applicability of this model for explaining XPS angular distributions, we show in Fig. 3(b) a (001) stereographic projection on which has been placed shaded bands of uniform intensity with $2\theta_{hkl}$ widths appropriate to the low-index planes mentioned. The positions and approximate widths of the experimental maxima along the [001], ⟨110⟩, and ⟨211⟩ directions are well predicted by this model (which implicitly neglects any changes in intensity due to purely instrumental effects). The full widths at half maximum intensity of certain peaks in the polar angular distribution curves also have magnitudes comparable to the one or more $2\theta_{hkl}$ values that Figs. 3(a) and 3(b) predict to be involved, especially if effects due to instrumental angular broadening are considered. For example, the widths of several prominent peaks have been derived from Fig. 2 relative to a smooth-curve background and these are given together with the direction along which each peak maximum occurs as follows: peaks 1—6.0°, [111]; peaks 5—6.8° [001]; peaks 6—7.6°, [011]; and peaks 10—6.0°, [001]. The structures observed in the outer contours of Fig. 3(a) such as those with value 10 are also in agreement with the qualitative predictions of Fig. 3(b) associated with the three lowest-index planes.

The intensity maxima observed near the ⟨221⟩, ⟨310⟩, and ⟨311⟩ directions are, on the other hand, not simply connected with the bands expected for the three lowest-index sets of planes. As judged by decreasing interplanar spacing [or equivalently, $(h^2+k^2+l^2)^{-1/2}$], the next set which might be involved is {311}, with $\theta_{311}=7.7°$. As an indication of the positions of the centers of the Kikuchi bands associated with these planes, dotted lines are shown in the lower half of Fig. 3(b). (The pattern in the upper half is obtained simply by reflection of that in the lower half.) The {311} bands are thus predicted to intersect and thus to tend to produce intensity maxima at eight points in a starlike pattern surrounding and rather close to [001]. The four intersections along {200} planes should occur along ⟨310⟩ directions, or at 18.4° from [001]; this value agrees very well with the average position of the four corresponding experimental peaks in Fig. 3(a), which is found to be 19.1° from [001]. (These peaks correspond to those numbered 8 in Fig. 2.) The four intersections along {220} planes are predicted to occur at 19.5° from [001], again in very good agreement with the mean experimental separation of 19.7°. (These experimental peaks are noted as 3 in Fig. 2.) Additional band intersections involving {311} are also expected to be found near, but not exactly along, the ⟨221⟩ directions, thereby at least partially explaining the intensity maxima observed very close to ⟨221⟩. Thus, by including only planes for which $h^2+k^2+l^2 \leq 11$, it is possible to explain most of the major features noted in Figs. 2 and 3(a).

If, in addition, the effects of bands associated with the next two higher-index planes {331} ($\theta_{331}=10.1°$) and {420} ($\theta_{420}=10.4°$) are considered, it is furthermore predicted that intersections and thus maxima should occur directly along ⟨221⟩, as well as at positions near ⟨211⟩ along the {111} bands. These predictions thus further account for the maxima noted along ⟨221⟩ in Fig. 3(a), as well as for the elongation of the intensity peaks observed near ⟨211⟩ along the direction of the {111} planes. Qualitatively, there is thus very good agreement between experiment and the approximate systematics expected for Kikuchi bands.

Detailed theoretical calculations of such single-crystal effects on XPS intensities have not been carried out previously, although McRae[8] has discussed a phenomenological model for them. A more accurate description of these effects will no doubt involve the inclusion of multiple-scattering effects such as is done in current dynamical analyses of either LEED data[14] or extended x-ray absorption-edge fine-structure (EXAFS) experiments.[15] In particular, XPS emission from a localized core level is identical to the basic transition occurring in EXAFS, although the final-state energy in a typical XPS experiment is somewhat higher than those of most interest in EXAFS.

B. Angular-dependent valence fine structure

As a final point, we comment qualitatively on the possible relationships existing between two separate effects noted in angular-dependent XPS studies of single-crystal Au: (i) the variation of energy-integrated valence-spectrum intensities with angle, as discussed in Sec. II A (cf. Fig. 2), and (ii) the angular dependence of the *relative* intensities and positions of various individual features in the d-band-dominated valence spectrum, as observed previously.[3,4,16] Figure 4 presents Au valence spectra obtained in this study at several closely-spaced angles along a given polar scan, and pronounced changes in the fine structure are evident.

A complete understanding of both of these effects

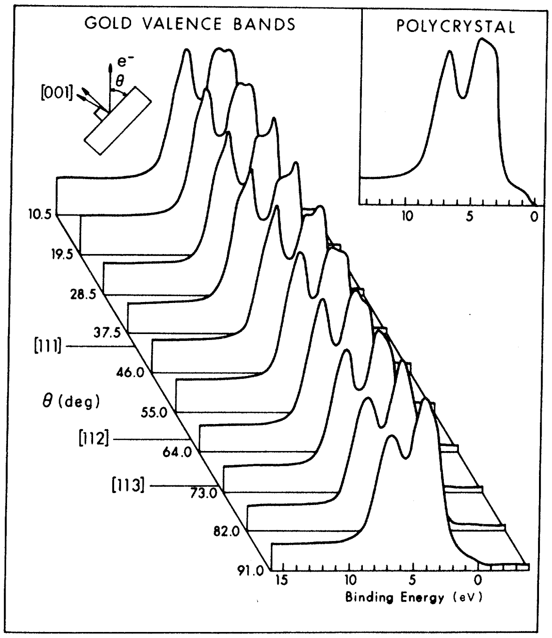

FIG. 4. Gold valence-band spectra are shown for various emission angles in a single polar scan. The locations of certain low-index directions are indicated, and the scan was made in the same plane as that for curves *A* in Fig. 2. The inset shows a polycrystalline spectrum for comparison. All spectra have been normalized to a constant maximum height. (See also Refs. 3 and 4.)

within the context of a single model will no doubt involve a one-step description of the photoemission process that includes the presence of the surface, as well as both bulk and surface secondary scattering phenomena in the final state. Although models of this type have been discussed previously,[17] no detailed numerical calculations relevant to the present case have been carried out. At a somewhat simpler level very close to the often-used three-step model of photoemission,[18] it is possible, however, to self-consistently explain the observed systematics of the two effects.

The angular-dependent valence-spectrum fine structure for Au has been successfully analyzed in terms of a direct-transition model[3,4] that is closely related to that used in prior angular-dependent ultraviolet photoemission (UPS) studies.[17,19] This model has been discussed in detail elsewhere,[3,4] but, in brief review, it yields a wave-vector selection rule of the form $\vec{k}^i + \vec{g} + \vec{k}_{h\nu} = \vec{k}^f$, in which $\vec{k}^i$ is the initial-state wave vector in a reduced-zone representation, $\vec{g}$ is a reciprocal lattice vector, $\vec{k}_{h\nu}$ is the (non-negligible) photon wave vector, and $\vec{k}^f$ is the photoelectron wave vector. The strength of each direct transition will be proportional to the square of a matrix element between the initial and final states. A free-electron (plane-wave) final state is also assumed for the XPS photoelectron. The wave-vector selection rule can then be used to determine the $\vec{k}^i$ associated with each free-electron $\vec{k}^f$ lying in the finite observation cone of the spectrometer, and a knowledge of the initial-state band structure $E^i(\vec{k}^i)$ then specifies the allowed distribution of final photoelectron energies. If the matrix elements associated with the various direct transitions are assumed to be approximately constant, a direct prediction of angular-dependent valence spectra can be made in this way. Good agreement is found between such calculations and XPS valence data for both Au (Ref. 3) and Cu.[20] The additional effect of angular-dependent matrix elements has also been found to yield theoretical results in agreement with some aspects of angular-dependent XPS valence spectra from Au and Ag.[16]

The question thus arises as to whether the simple free-electron final state assumed in the direct-transition model is consistent with the more complex final state expected as a result of the multiple scattering effects producing Kikuchi phenomena. The XPS data obtained to date for these two types of effects can be explained if it is assumed that the x-ray photoemission process approximately separates into an initial direct transition ($\vec{k}^i \rightarrow \vec{k}^f$) followed by secondary scattering ($\vec{k}^f \rightarrow \vec{k}^{f\prime}$) that is dependent primarily on $\vec{k}^f$.[21] Secondary scattering would thus act to mix other plane waves into the final-state description, so as to produce, for example, the secondary diffraction cones discussed by Mahan,[17] as well as Kikuchi-like effects. If constant matrix elements are further assumed, then the energy-integrated valence intensity before secondary scattering from noble metals with a filled set of *d* bands below the Fermi energy is predicted to be very nearly constant with angle. This is because the *d* bands contribute most of the XPS spectral intensity and all observed $\vec{k}^f$ values can be projected back via suitable choices of $\vec{g}$'s to yield $\vec{k}^i$'s associated with occupied initial states in each *d* band. Such a constant intensity with angle before secondary scattering is thus equivalent to the situation expected for core-level emission. (Note that the angle α in Fig. 1 is assumed to be constant, and so is not involved in the angular dependence of either core or valence intensities.) Inasmuch as the magnitude of $\vec{k}^f$ is very nearly the same for all valence levels and high-lying core levels, it would thus further be expected that secondary scattering would tend to modulate the intensities at all points within the spectra from such levels by approximately the same factor at a given angle without, for example, introducing new structure in the valence spectra. This prediction is thus consistent with the essentially identical energy-integrated $4d$, $4f$, and valence angular distributions shown in Fig. 2.

Even if matrix-element anisotropies are a significant factor in producing valence fine-structure changes with angle, it is also possible to use the same two-step model to explain the observed phenomena, provided that a tight-binding description of the noble-metal d bands neglecting s,p hybridization is adopted. (Such a model has, for example, been used previously in deriving possible matrix-elements effects.[16]) Such a description would suggest that the energy-integrated intensity over all d bands should have a single-crystal angular distribution very close to that from any filled high-lying core subshell, as is found to be the case. That is, in integrating intensities over all d bands for a given emission direction, the net result will involve summations over full sets of m_l values analogous to those producing core level intensities.

Although this model is no doubt somewhat oversimplified in its two-step separation, it is consistent with the available data, and may serve as a useful first-order approximation in subsequent experimental and theoretical studies of such effects.

IV. CONCLUSIONS

The overall systematics of angular distributions of energy-integrated XPS intensities from gold $4d$, $4f$, and valence levels are qualitatively very well described in terms of Kikuchi-band effects that are primarily controlled by the final-state character of the process. A plausible relationship between such angular distributions and the angular-dependent changes noted previously in XPS valence-spectrum fine structure has also been discussed. More quantitative experimental and theoretical studies will be necessary to fully characterize these effects, including theoretical calculations utilizing dynamical diffraction theory. A detailed understanding of such phenomena is essential for the quantitative interpretation of XPS data from any single crystal specimen.

The support of the National Science Foundation (Grant Nos. GP-38640X and MPS75-05055) and the Alfred P. Sloan Foundation is gratefully acknowledged. The assistance of J. A. Schoeffel in performing LEED measurements and of J. D. Tuthill and R. E. Johnson in deriving intensity contours is also appreciated.

---

†Supported by the Alfred P. Sloan Foundation.

[1] K. Siegbahn, U. Gelius, H. Siegbahn, and E. Olsen, Phys. Lett. A 32, 221 (1970); Phys. Scr. 1, 272 (1970).

[2] C. S. Fadley and S. Å. L. Bergström, Phys. Lett. A 35, 375 (1971); and in *Electron Spectroscopy*, edited by D. A. Shirley (North Holland, Amsterdam, 1972), p. 233.

[3] R. J. Baird, C. S. Fadley, and L. F. Wagner, Discuss. Faraday Soc. 60, 143 (1975); and Phys. Rev. Lett. 37, 111 (1976).

[4] C. S. Fadley, in *Progress in Solid State Chemistry*, edited by G. A. Samorjai and J. O. McCaldin (Pergamon, New York, 1976), Vol. 11, p. 265.

[5] J. Brunner and H. Zogg (private communication); H. Zogg, Ph.D. thesis (Eidgenössische Technische Hochschule, Zürich, 1974).

[6] J. M. Hill, D. G. Royce, C. S. Fadley, and F. J. Grunthaner, Chem. Phys. Lett. (in press).

[7] N. E. Erickson (private communication).

[8] E. G. McRae, Surf. Sci. 44, 321 (1974), and references therein.

[9] R. Baudoing, R. M. Stern, and H. Taub, Surf. Sci. 11, 225 (1968), and references therein.

[10] R. J. Baird and C. S. Fadley, paper presented at the Northwest Regional Meeting of the American Chemical Society, Honolulu, June, 1975 (unpublished); J. Electron Spectrosc. (in press).

[11] C. S. Fadley, R. J. Baird, W. Siekhaus, T. Novakov, and S. Å. L. Bergström, J. Elect. Spect. 4, 93 (1974).

[12] M. Mehta and C. S. Fadley, Phys. Lett. A 55, 59 (1975).

[13] We have throughout used the standard notation for directions and planes: ( ) equals a definite plane, { } equals a set of symmetry-related planes, [ ] equals a definite direction, and ⟨ ⟩ equals a set of symmetry-related directions.

[14] See, for example, C. B. Duke, Jpn. J. Appl. Phys. Suppl. 2, 641 (1974); J. B. Pendry, *Low Energy Electron Diffraction* (Academic, London, 1974), and references therein.

[15] E. A. Stern, Phys. Rev. B 10, 3027 (1974); C. A. Ashley and S. Doniach, Phys. Rev. B 11, 1279 (1975).

[16] F. R. McFeely, J. Stöhr, G. Apai, P. S. Wehner, and D. A. Shirley, Phys. Rev. B (to be published); K.-F. Berggren and F. Martino (private communication).

[17] G. D. Mahan, Phys. Rev. B 2, 4334 (1970); W. L. Schaich and N. W. Ashcroft, Phys. Rev. B 3, 2452 (1970); P. J. Feibelman and D. E. Eastman, Phys. Rev. B 10, 4932 (1974).

[18] C. N. Berglund and W. E. Spicer, Phys. Rev. 136, A1030, A1044 (1964).

[19] P. O. Nilsson and L. Ilver, Solid State Commun. 17, 667 (1975); L. Ilver and P. O. Nilsson, *ibid.* 18, 677 (1976).

[20] L. F. Wagner, Z. Hussain, C. S. Fadley, and R. J. Baird, Solid State Commun (in press).

[21] In essence, this model thus combines the second two steps of the three-step model (transport to the surface and escape from the surface) into one, and adds the further simplification of a free electron $\vec{k}^f$.